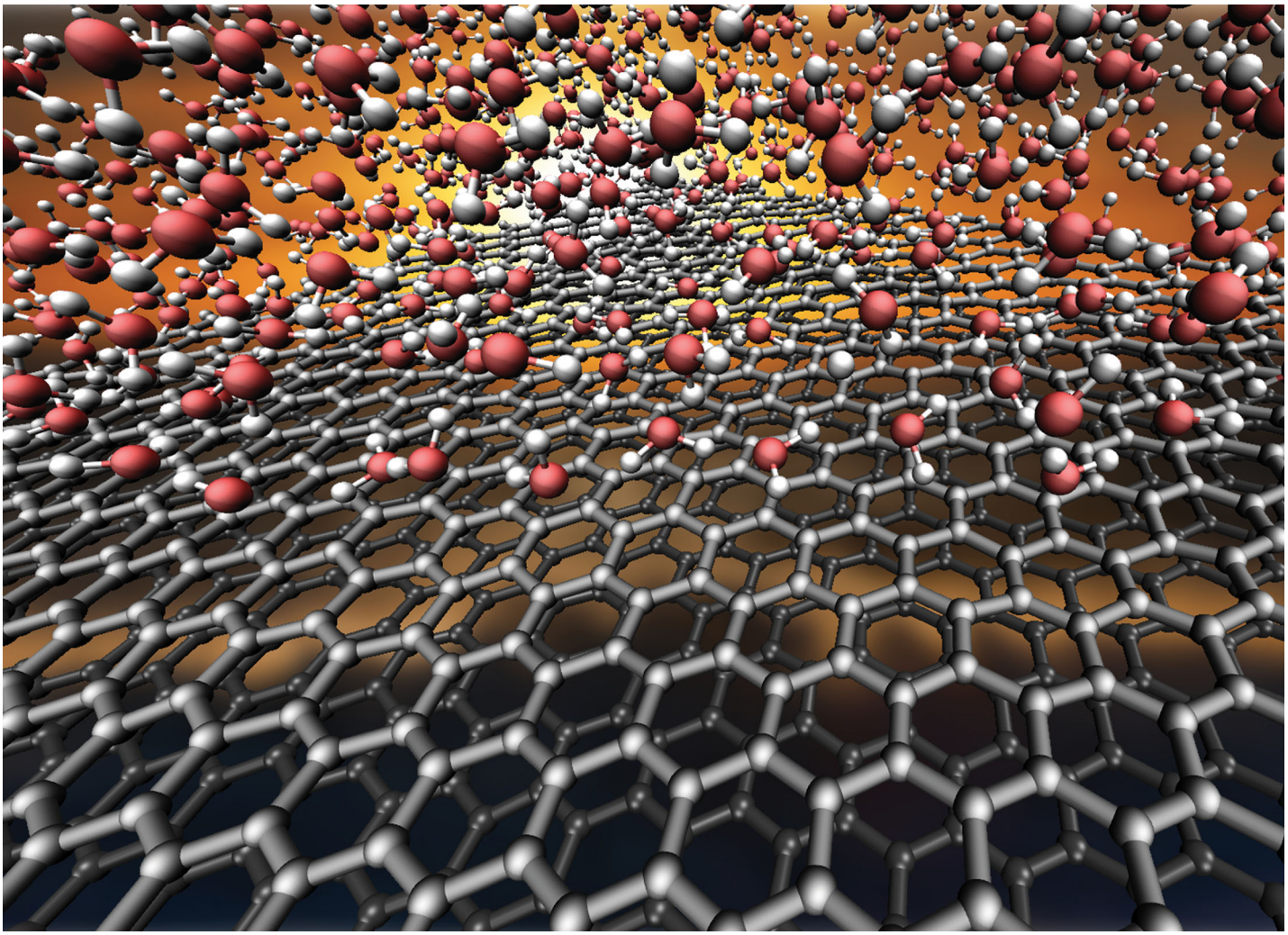

Highlighting results from research conducted by E. Wagemann under the supervision of Prof. H. A. Zambrano and Prof. J. H. Walther (DTU) in the Computational Nanofluidics group, Department of Chemical Engineering (FI), Universidad de Concepcion, Chile.

Slip divergence of water flow in graphene nanochannels: the role of chirality

In this work a computational study of water flow anisotropy in graphene nanochannels finds a constant slip length up to a critical value of the shear stress of 0.4 Mpa. As slip divergence occurs, the flow is chirality dependent which means that the slip velocity varies up to 10% with the particular flow orientation in the channel.

As featured in:

See Harvey A. Zambrano *et al.*, *Phys. Chem. Chem. Phys.*, 2017, **19**, 8646.

ROYAL SOCIETY OF CHEMISTRY

rsc.li/pccp

Registered charity number: 207890

PCCP

COMMUNICATION

View Article Online
View Journal | View Issue

Cite this: *Phys. Chem. Chem. Phys.*, 2017, **19**, 8646

Received 12th November 2016,
Accepted 1st February 2017

DOI: 10.1039/c6cp07755b

rsc.li/pccp

Slip divergence of water flow in graphene nanochannels: the role of chirality†

Enrique Wagemann,[a] Elton Oyarzua,[a] Jens H. Walther[bc] and Harvey A. Zambrano*[a]

Graphene has attracted considerable attention due to its characteristics as a 2D material and its fascinating properties, providing a potential building block for nanofabrication. In nanochannels the solid–liquid interface plays a non-negligible role in determining the fluid dynamics. Therefore, for an optimal design of nanofluidic devices, a comprehensive understanding of the slippage in a water flow confined between graphene walls is important. In nanoconfinement, experimental and computational studies have found the slip length to increase nonlinearly when the shear rate is larger than a critical value. Here, by conducting molecular dynamics simulations, we study the influence of the graphene crystallographic orientation on the slip boundary conditions inside a nanoslit channel. The flow in channels with heights of 2.0, 2.4 and 2.8 nm is driven parallel to the zig-zag and arm-chair crystallographic directions. We extract flow rates, velocity profiles, slip velocities and slip lengths. The slip velocity displays a linear relationship to the shear stress up to a critical value, which is not size dependent. Moreover, the slip length is found to be shear stress dependent above a critical shear stress value of 0.4 MPa. Furthermore, our results indicate that after this critical shear stress is reached, the flow rates are significantly influenced (up to 10%) by the particular orientation of the graphene topology.

1 Introduction

Nanoscale fluid dynamics has attracted considerable interest as part of the current fascination with nanotechnology and the consequent attempt to design and fabricate integrated nanofluidic devices such as Lab-On-a-Chip (LOC) units and nanoscale sensor systems.[1–5] The flow of water in nanoconfinement has been extensively studied;[6–10] however, many fundamental questions remain open and are yet the subject of intense debate. It is well recognized that the physics of fluids at the nanoscale is dominated by the large surface area-to-volume ratio inherent to this scale;[10–15] thus interfacial transport phenomena greatly impact the fluid behavior.[16–19] Technologically, nanofluidics has become interesting as the basis for further miniaturization of microfluidic devices. Indeed, the possibility of extending the LOC concept to the nanoscale, the potential role of carbon nanostructures as highly efficient fluid conduits,[6,10,14,20–22] and the development of novel drug storage units, biochemical devices, nanofilters and nanosensors are paradigmatic examples of the importance of nanofluidics. Graphene is a carbon allotrope which consists of a single plane sheet of carbon atoms arranged in a symmetric hexagonal lattice.[23] The chirality of a graphene sheet is determined by the in-plane orientation of the hexagonal lattices.[24] The isolation of a single sheet of graphene[23,25] has led to the fast development of many promising applications[26–29] including its potential utilization in a wide variety of functional parts in nanofluidic devices.[30–32] Therefore, a comprehensive understanding of transport of water confined inside or in contact with graphene layers is important for the design of nanofluidic devices.[33] In macroscale fluid dynamics, the multi-centenary assumption of a no-slip boundary condition at solid walls is at the core of our understanding of fluid transport.[34] Nevertheless, over years persistent doubts have been expressed.[10,33,35,36] Indeed, studies of flow in micro- and nano-confinement have found a constant slip length in Newtonian liquids.[37] Furthermore, recent investigations have concluded that the amount of slip depends on the local shear rate at the solid surface;[7,38–40] therefore, the slippage is velocity dependent. Moreover, the wettability of graphene with respect to water is still not well understood[41–44] and is a topic widely investigated in recent years. Furthermore, faster than expected water flow rates have been observed in carbon nanotubes and graphene channels,[10,15,20,21] which have been attributed to an extremely low friction of water with the atomistically smooth walls.[9,45] This low viscous drag makes graphene a promising coating material to mitigate hydrodynamic losses in nanochannels. In this study, we conducted large scale and long time (more than 60 ns) atomistic simulations to investigate the water flow dynamics inside graphene nanochannels.

[a] *Universidad de Concepcion, Concepcion, Chile. E-mail: harveyzambrano@udec.cl; Tel: +56 41266 1468*
[b] *Technical University of Denmark, Copenhagen, Denmark*
[c] *Chair of Computational Science, ETH Zurich, Zurich, Switzerland*
† Electronic supplementary information (ESI) available. See DOI: 10.1039/c6cp07755b

Specifically, the effects of channel height and graphene chirality on the amount of slip are investigated by computing flux, flow rates, critical shear stress, friction coefficients and flow enhancement. Here, we consider how a Newtonian fluid flow inside a graphene channel responds to variations in the lattice orientation of the confining graphene walls. Our results provide insights into prediction of fluid transport in hydrophobic nanostructures, which is essential to develop functional nanofluidic devices.

2 Methodology

To study the hydrodynamic properties of water confined in graphene nanochannels we conducted a series of Equilibrium and Non-Equilibrium Molecular Dynamics (NEMD) simulations. All simulations were carried out using the FASTTUBE MD package, which has been used extensively to study liquids confined inside carbon nanotubes and silica channels.[11–13,46–48] Our systems confine water between two walls of graphene. The walls consist of parallel AB-stacked bilayers of graphene. A snapshot of the studied systems is shown in Fig. 1A, where h corresponds to the channel height, which is defined as the mean distance between the centres of mass of the carbon atoms in the innermost graphene layers. An orthorhombic box is used with periodic boundary conditions in the x and y directions, while free space conditions are applied in the z direction. The x and y dimensions are chosen to minimize artificial strain[49] in the graphene sheet due to the periodic boundary conditions. Two external fixed graphene layers which do not interact with the water molecules are implemented. These layers are added to confine the system, thus avoiding the necessity for fixed carbon atoms in the inner layers interacting with water. To achieve an internal pressure of 1 bar, a size dependent number of water molecules are placed between the graphene walls. Subsequently, one of the graphene walls is used as a piston to impose the target pressure and then the carbon atoms in the most external layer are fixed to reproduce a channel with the required mean height. We took special care of the confinement of the system, as the internal pressure is known to affect the slip length.[50,51] It should be noted that the two inner graphene sheets are maintained flexible and free in all directions during the simulations. Density profiles, presented in Fig. 1B, show bulk and interfacial densities in good agreement with previous works[46,49] and exhibit no difference between the correspondent armchair (AC) and zig-zag (ZZ) cases. After imposing an axial force on the confined water, an initial sliding occurs between the graphene layers, which subsequently equilibrate in an A–B–A arrangement[52] as the friction stops the sliding.

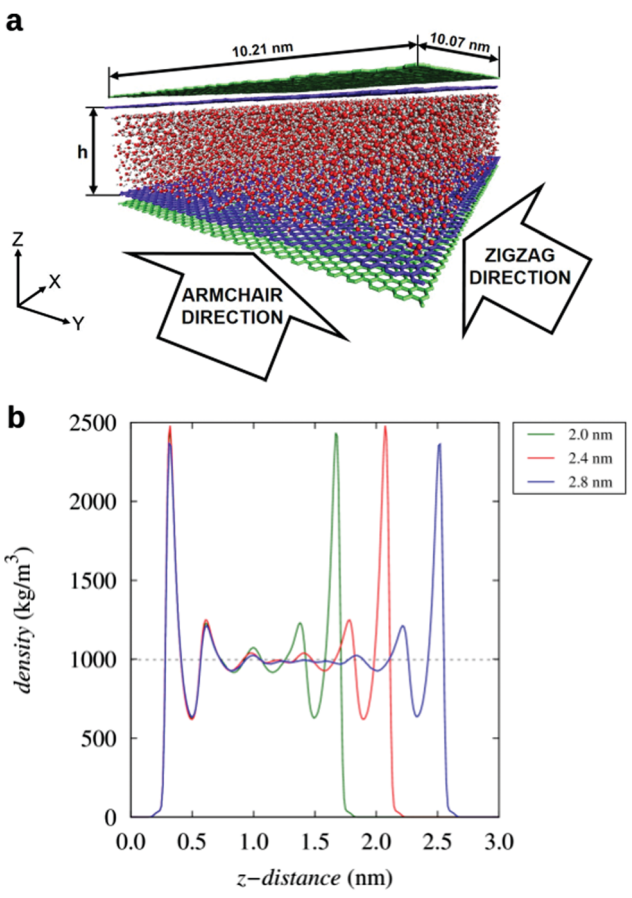

Fig. 1 (A) Snapshot of the studied systems. Water is confined between two walls conformed by two graphene sheets each (green and blue). Two additional fixed graphene layers (not shown) that don't interact with water are used to confine the system. (B) Density profiles for the studied channel heights.

The water molecules are described using the classical SPC/E model.[53] In the graphene sheet, the carbon–carbon valence forces are described using Morse, harmonic angle and torsional potentials.[13,47,48] A nonbonded carbon–carbon 12-6 Lennard-Jones potential with parameters $\varepsilon_{CC} = 0.4396$ kJ mol^{-1} and $\sigma_{CC} = 0.3851$ nm is used to describe the vdW interaction between the carbons within different graphene layers. The water–carbon interaction is modelled by a Lennard-Jones potential with parameters obtained by Werder *et al.*[46] to recover the macroscopic contact angle of water on graphite of 86°. Momentum transfer from the solid to the liquid is known to affect slip length;[54] thus in order to avoid the direct application of a heat bath to the fluid molecules, viscous Joule heat is subtracted from the system by coupling a Berendsen thermostat[55] to the carbon atoms with a weak coupling constant of 0.1 ps to a temperature of 300 K. We measured the water temperature in each system after the steady state was reached to ensure effective heat removal, obtaining positive results. Coulombic and van der Waals interactions are truncated at 1 nm.[13,46,47,50] The leap-frog integration algorithm with a time step of 2 fs is used to integrate the equations of motion. Poiseuille like flow is generated by imposing a constant force field on all water molecules inside the channel. The direction of the external force field is systematically changed to study flow in both AC and ZZ directions. Simulations are conducted for more than 60 ns, extracting data after the first 5 ns.

3 Results

This study reports about water flow in slit graphene channels with heights of 2.0, 2.4 and 2.8 nm. We varied systematically the external field to impose accelerations from 5×10^{10} to 1.6×10^{12} m s^{-2} in the direction towards the ZZ and AC crystallographic orientations of the graphene walls, respectively.

It should be noted that although the pressure gradients, corresponding to the studied external fields, have not been achieved experimentally, new and promising techniques are being developed to achieve high pressure gradients at the nanoscale.[56] Flow velocity and density profiles across the channels are computed using the binning method.[50] The velocity profiles are shown in Fig. 2A and exhibit the expected plug-like flow, displaying high slip velocities. Due to the extremely low curvature of the velocity profiles and the uncertainty related to the thermal noise, slip velocity is estimated from the average flow velocity across the channel. For pressurized water flow in nanochannels with graphitic walls, a plug-like flow is expected as numerous studies have reported this behavior.[15,37,49,57–60] Nevertheless, the flow velocities as a function of channel height depicted in Fig. 2B show that a parabolic flow profile can still be recovered as a greater signal to noise ratio is achieved by imposing higher external fields. Therefore, the parabolic shape of the profiles suggests that viscosity still has an influence on the flow; thus in graphene channels, the flow can be described using a modified Hagen–Poiseuille model.[61,62] Moreover, as higher external fields are applied, the velocity profiles shown in Fig. 2A reveal that higher velocities are computed for flow imposed along the AC direction, which implies lower slip velocities for the corresponding cases with flow along the ZZ direction. Furthermore, using the method reported by Ritos *et al.*[59] we computed the water flux and subsequently, from the corresponding flux values, the volumetric flow, as shown in Fig. 2C. Under higher imposed external fields, volumetric flow rates confirm that different flow velocities are achieved for the AC and ZZ flow directions. Moreover, Fig. 2C shows that the volumetric flow rate displays a linear response to the imposed external field up to a critical value. Indeed, as the critical value of the external field is reached, the flow rates become flow direction dependent, which indicates that slip velocity (v_s) is chirality dependent after a critical value of flow velocity. In order to gain insight into the relationship between flow rates and the particular flow direction, we refer to the concepts of enhancement (ε) and slip length (l_s), criteria widely used to compare flows with a significant slippage.[15,21,37,38,50,63,64] The ε corresponds to the ratio between the computed flow and the theoretical Poiseuille flow. Our theoretical flow rates were calculated by feeding the bulk viscosity for the SPC/E model[65] into the no slip Hagen–Poiseuille solution of the Navier–Stokes equations, wherein the fluid velocity at the wall vicinity is assumed to be equal to zero. Slip length calculations follow the P5 procedure reported by Kannam *et al.*[37] This method requires no fit of the computed flow velocities to a theoretical velocity profile, as flow in graphene channels displays very low curvature profiles and is very sensitive to thermal noise.

In Fig. 3 slip length as a function of the shear rate $\left(\dot{\gamma} = \frac{v_s}{l_s}\right)$ is shown for all cases. A constant value of the slip length around 50 nm is computed for shear rate values lower than 6×10^8 s^{-1}. After this critical value of the shear rate, the slip length diverges from a linear behavior. We noted that divergence in the slip length values was first reported by Thompson and Troian.[38] In their work, they investigated the shear rate effect on the slip length by conducting MD simulations of a simple Newtonian fluid under a Couette flow regime. While systematically increasing the wall velocity, they found a slip length dependence on the applied shear rate. They reported no change in the bulk viscosity; therefore, the shear dependence is not related to a non-Newtonian behavior in the bulk zone of the fluid. Indeed, they proposed that the value of the shear rate at which the nonlinear behavior of slip occurs is determined by the corrugation of the potential surface

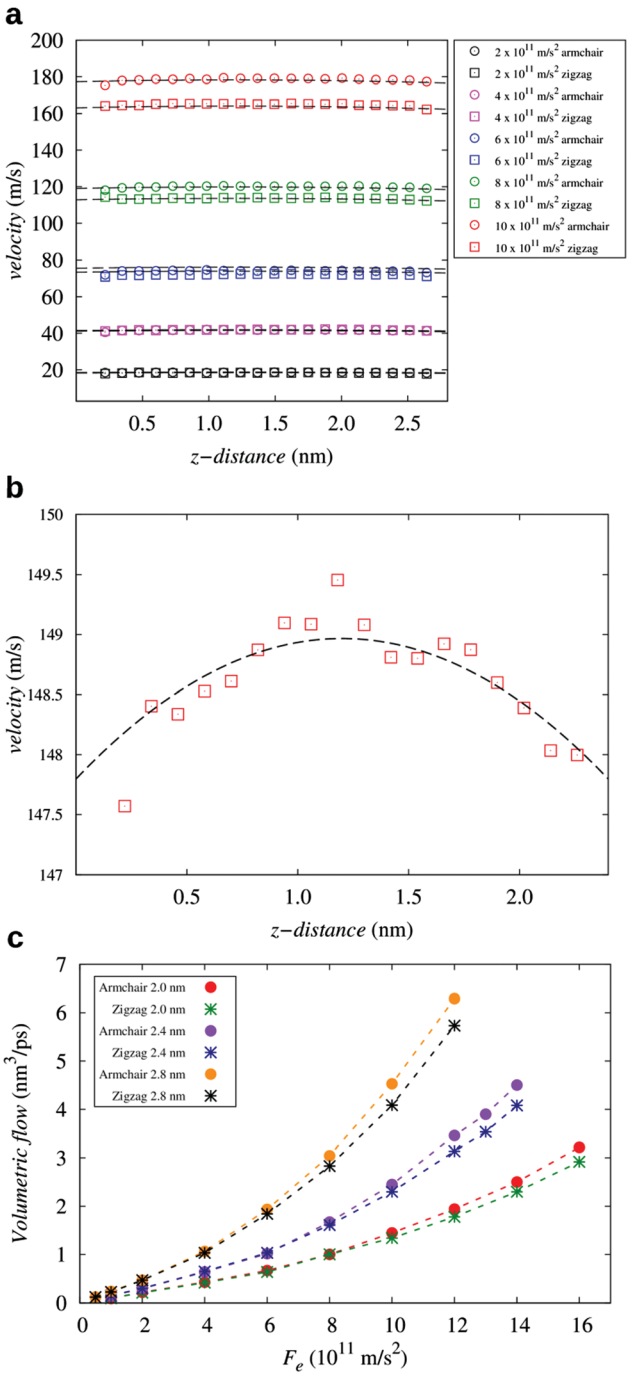

Fig. 2 (A) Velocity profiles for the different applied external fields for the 2.8 nm height case. Black dashed lines represent the modified Hagen–Poiseuille model fit. (B) Velocity profile for the 2.4 nm height case with an applied external field of 1.2×10^{12} m s^{-2} in the zigzag direction. (C) Volumetric flow as a function of the applied external field for each studied case.

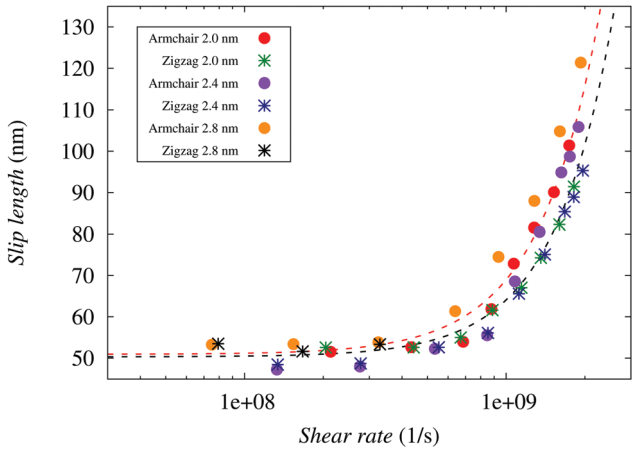

Fig. 3 Slip length as a function of the shear rate. For low shear rates a constant slip length of approximately 50 nm is observed up to a critical shear rate value, where divergence is observed. A difference in the slip length between armchair and zigzag is observed beyond this value. The dashed lines correspond to a power law fit to the AC (red) and ZZ (black) cases and serve as a visual aid.

at the fluid–solid interface. This work has been a subject of controversy during the last two decades. Indeed, several studies have confirmed this behavior,[66–69] whereas many others have reported no agreement with the slip divergence.[54,63] Nevertheless, all these studies agree that the slip divergence depends on the rate of momentum transfer between the solid surface and the fluid. In our simulations, to ensure a proper description of the graphene–water momentum transfer (with case 1 as the reference case), we varied systematically the graphene interlayer distance by using the carbon–carbon intermolecular potentials parametrized by Saito[70] (case 2) and by Girifalco[71] (case 3). In both cases, the thermostat is applied only to the carbon atoms rather than to the fluid molecules. Moreover, to test the Joule heat extraction, we conducted simulations with the thermostat coupled simultaneously to the water molecules and to the carbon atoms (case 4) and also with the thermostat connected to the water molecules while maintaining the carbon atoms rigid (case 5). Each case has the same number of water molecules confined in graphene channels with heights of 2.8 nm. An external field of 10^{12} m s^{-2} was applied in both crystallographic directions. The results of these simulations are listed in Table 1. We note that the flow properties exhibit good agreement for the cases with active carbon atoms. Nevertheless, in the case with rigid carbon, a considerably shorter slip length was computed, at least 20% lower than the ones computed in the cases with active carbon atoms as listed in Table 1. Furthermore, for all cases, significant differences in the slip lengths are computed for the flow along the ZZ and AC crystallographic directions as listed in Table 1.

Previous works have explored how slip occurs at the molecular level.[34,38,45,66–69,72] In particular, Martini[66] and Wang *et al.*[67] studying Couette and Poiseuille flow in nanochannels proposed a series of molecular mechanisms describing the slip development. They found that the slip is different depending on the magnitude of the shear stress and the capacity of the fluid molecules near the wall to overcome the potential energy corrugations projected

Table 1 Slip length for a 2.8 nm height channel with an applied external field of 10×10^{11} m s^{-2} in both directions for each case

	Slip length (nm)	
Case	Armchair	Zigzag
1	106.8	96.4
2	104.3	95.1
3	104.3	95.1
4	109.8	98.3
5	80.3	74.2

by the wall atoms. That is, slip divergence occurs when the shear reaches a critical value. The results of Martini and Wang under high shear stress agree with the results of Thompson and Troian[38] of Couette flow of a Newtonian fluid. In the present work, τ is calculated from the value of the external force, the number of water molecules, the molecular mass and the surface area as $\tau = Nma/2A$. Our results, shown in Fig. 4A, are in line with these studies, as after a critical value of τ, around 0.4 MPa, the slip length appears to diverge, caused by the nonlinearity of v_s with τ. On the other hand, for values of τ below the critical shear, our results indicate a constant friction coefficient (λ), which is expected for a Newtonian flow with constant slip length, as $\tau = -\lambda \cdot v_s$. Furthermore, when slip divergence is reached, a significant difference arises between the flows computed in the armchair and the zigzag crystallographic directions, as shown in Fig. 4A and B.

Chirality dependent water flow in CNTs has been previously reported.[13,73,74] Falk *et al.*[73] studied the relationship between the slip length estimated from the carbon–water friction coefficient, and the corrugation of the carbon surface energy for different CNT radii. They found that as the CNT radius decreases, the energy corrugation felt by a water molecule becomes smoother and consequently the friction coefficient ($\lambda = -\tau/v_s$) decreases nonequally for the AC and ZZ CNTs below a critical radius of 3 nm. For flow in graphene channels at relatively low shear rates, Falk *et al.*[73] found the friction to be independent of the flow orientation. In the present work, the slip velocity and the volumetric flow ratio as a function of shear stress depicted in Fig. 4A and B exhibit an isotropic flow for shear stress below a critical value of 0.4 MPa in agreement with Falk *et al.*[73] Moreover, it is noted that below this critical shear stress, v_s depends linearly on τ; therefore, the friction coefficient λ is constant for flow in both crystallographic directions. Nevertheless, in Fig. 4A as the critical shear stress value is reached, the slope of the function v_s *vs.* τ increases, which means that the friction coefficient λ starts to decrease, resulting in slip divergence. In the present study, as the slip divergence occurs, anisotropic water flow is observed, which means that the flow becomes graphene chirality dependent as depicted in Fig. 4A. Indeed, as confirmed in Fig. 4C a reduction in the friction coefficient λ leads to the observed chirality dependent flow. This behavior is consistent with the results found by Tocci *et al.*[45] for water flow on graphene and hexagonal boron nitride sheets. Performing first principles simulations, they found that although for the two sheets the interface presents a very similar structure, the friction coefficients are significantly different. Moreover, in a recent

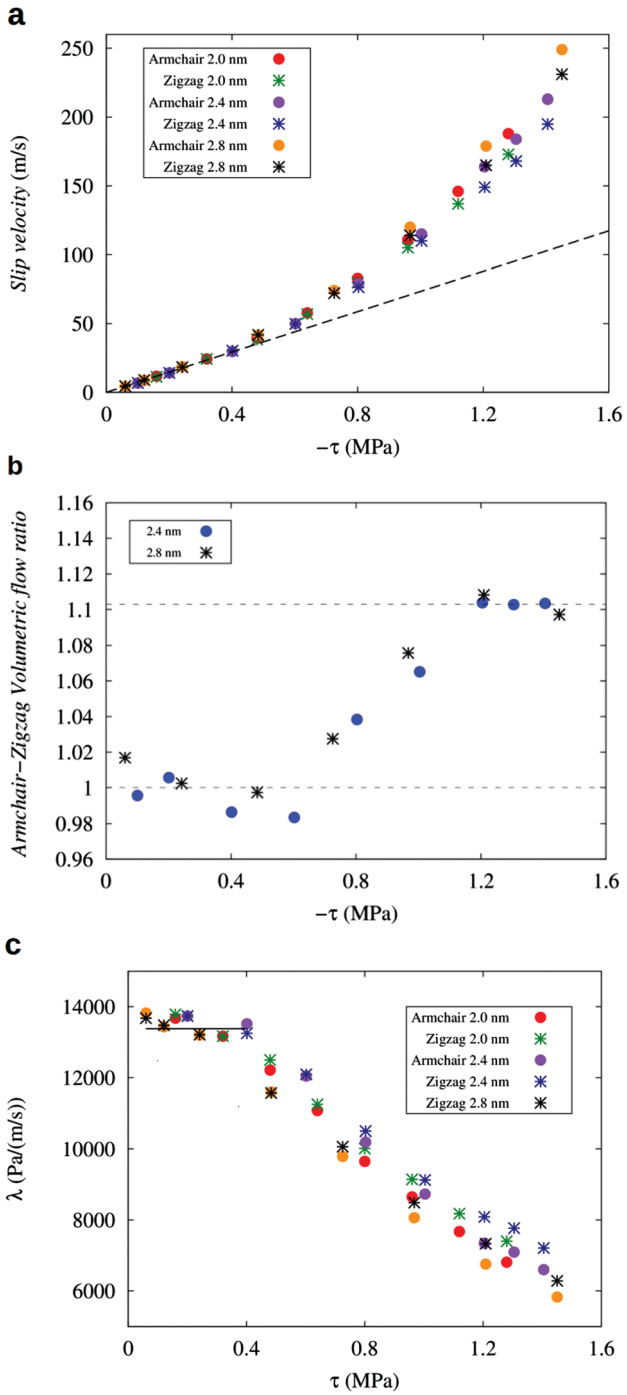

Fig. 4 (A) Slip velocity as a function of the shear stress. Linear dependence between shear stress and slip velocity is found up to a divergence point. (B) AC–ZZ flow ratio *vs.* shear stress. Three flow regimes are found: AC and ZZ equal friction coefficient (FC) (equal AC–ZZ flow), a transient regime, and a third regime in which the ratio of AC FC and ZZ FC converges to a constant value around 1.1. (C) Friction coefficient as a function of shear stress. The black line represents the mean λ for the nondivergence zone.

experimental study, Secchi *et al.*[10] found similar results for flow in CNTs and boron nitride nanotubes that are crystallographically similar. They attributed the differences observed to subtle atomic-scale details of the solid–liquid interface. Furthermore, we believe that anisotropic transport of water in graphene channels at high shear stress is the result of a lower energy dissipation at the wall–fluid surface which originates from a reduction in the momentum transfer at higher flow velocities. It has been reported that the momentum transfer decreases after slip divergence occurs, resulting in a weak friction flow dominated by the relative surface energy corrugation.[35,38] Specifically, the amount of slip increases with decreasing surface energy corrugation. In order to confirm the anisotropic fluid flow, we computed the AC/ZZ flow ratio as a function of τ as shown in Fig. 4B where a ratio equal to 1 is computed for the shear stress below the critical value. Subsequently, as slip divergence occurs, Fig. 4B shows that the AC/ZZ flow ratio starts to increase up to a constant value around 1.1, showing the existence of a transition regime wherein momentum transfer is still significant to determine the water flow rates. We believe that as the effect of the interfacial momentum transfer on the flow diminishes, the slip velocity becomes directly related to the surface energy corrugation felt by the water molecules. It should be noted that the surface energy corrugation on the graphene walls is inherently dependent on the particular ZZ or AC flow orientation.[74]

4 Conclusion

NEMD simulations were carried out to study flow anisotropy in pressure driven water transport in graphene channels. For low shear rates, a constant slip length of approximately 50 nm is found up to a critical value of the shear stress of *ca.* 0.4 MPa below which flow is not chirality dependent. As slip divergence occurs, the flow starts to be chirality dependent which means that the slip velocity varies up to 10% with the particular flow orientation, *i.e.* the armchair or zigzag crystallographic directions. We relate the anisotropic flow within the slip divergence zone to a reduction in the effect of the momentum transfer in the wall–fluid interface resulting in an enhanced effect of the surface energy corrugation felt by the interfacial water molecules.

Acknowledgements

The authors thank computational support from the Danish Center for Scientific Computing (DCSC) and from the National Laboratory for High Performance Computing (NLHPC). E. Wagemann thanks financial support from the Universidad de Concepcion under the REDOC scholarship program and from Centro CRHIAM Conicyt/Fondap Project 15130015. This research was partially funded by CONICYT under FONDECYT project no. 11130559. We also thank the partial financial support from the University of Concepcion under VRID project no. 21496651. The authors wish to acknowledge discussion with Andres Cordoba Uribe.

References

1 H. A. Stone, A. D. Stroock and A. Ajdari, *Annu. Rev. Fluid Mech.*, 2004, **36**, 381–411.
2 R. Daw and J. Finkelstein, *Nature*, 2006, **442**, 367.
3 C. D. Chin, V. Linder and S. K. Sia, *Lab Chip*, 2007, **7**, 41–57.
4 H. Craighead, *Nature*, 2006, **442**, 387–393.

5 C. Duan, W. Wang and Q. Xie, *Biomicrofluidics*, 2013, **7**, 1–41.
6 P. Kral and B. Wang, *Chem. Rev.*, 2013, **113**, 3372–3390.
7 L. Li, J. Mo and Z. Li, *Phys. Rev. E: Stat., Nonlinear, Soft Matter Phys.*, 2014, **90**, 033003.
8 L. H. Thamdrup, K. F. Persson, H. Bruus, A. Kristensen and H. Flyvbjerg, *Appl. Phys. Lett.*, 2007, **91**, 1–3.
9 S. Joseph and N. Aluru, *Nano Lett.*, 2008, **8**, 452–458.
10 E. Secchi, S. Marbach, A. Nigues, D. Stein, A. Siria and L. Bocquet, *Nature*, 2016, **537**, 210–213.
11 E. Oyarzua, J. H. Walther, A. Mejia and H. A. Zambrano, *Phys. Chem. Chem. Phys.*, 2015, **17**, 14731–14739.
12 N. K. Karna, E. Oyarzua, J. H. Walther and H. A. Zambrano, *Phys. Chem. Chem. Phys.*, 2016, **18**, 31997–32001.
13 H. A. Zambrano, J. H. Walther, P. Koumoutsakos and I. F. Sbalzarini, *Nano Lett.*, 2009, **9**, 66–71.
14 J. H. Walther, K. Ritos, E. Cruz-Chu, C. M. Megaridis and P. Koumoutsakos, *Nano Lett.*, 2013, **13**, 1910–1914.
15 S. K. Kannam, B. Todd, J. S. Hansen and P. J. Daivis, *J. Chem. Phys.*, 2013, **138**, 094701.
16 C. Bakli and S. Chakraborty, *Nano Lett.*, 2015, **15**, 7497–7502.
17 B. Ramos-Alvarado, S. Kumar and G. Peterson, *Phys. Rev. E*, 2016, **93**, 023101.
18 T. A. Ho, D. V. Papavassiliou, L. L. Lee and A. Striolo, *Proc. Natl. Acad. Sci. U. S. A.*, 2011, **108**, 16170–16175.
19 T. Q. Vo and B. Kim, *Sci. Rep.*, 2016, **6**, 33881.
20 J. K. Holt, H. G. Park, Y. Wang, M. Stadermann, A. B. Artyukhin, C. P. Grigoropoulos, A. Noy and O. Bakajin, *Science*, 2006, **312**, 1034–1037.
21 M. Majumder, N. Chopra, R. Andrews and B. J. Hinds, *Nature*, 2005, **438**, 44.
22 B. Radha, A. Esfandiar, F. Wang, A. Rooney, K. Gopinadhan, A. Keerthi, A. Mishchenko, A. Janardanan, P. Blake and L. Fumagalli, *et al.*, *Nature*, 2016, **538**, 222–225.
23 A. K. Geim and K. S. Novoselov, *Nat. Mater.*, 2007, **6**, 183–191.
24 C. Almeida, V. Carozo, R. Prioli and C. Achete, *J. Appl. Phys.*, 2011, **110**, 086101.
25 K. Novoselov, A. K. Geim, S. Morozov, D. Jiang, M. Katsnelson, I. Grigorieva, S. Dubonos and A. Firsov, *Nature*, 2005, **438**, 197–200.
26 S. Stankovich, D. A. Dikin, G. H. Dommett, K. M. Kohlhaas, E. J. Zimney, E. A. Stach, R. D. Piner, S. T. Nguyen and R. S. Ruoff, *Nature*, 2006, **442**, 282–286.
27 A. K. Geim, *Science*, 2009, **324**, 1530–1534.
28 X. Li, X. Wang, L. Zhang, S. Lee and H. Dai, *Science*, 2008, **319**, 1229–1232.
29 M. D. Stoller, S. Park, Y. Zhu, J. An and R. S. Ruoff, *Nano Lett.*, 2008, **8**, 3498–3502.
30 H. Li, L. Zou, L. Pan and Z. Sun, *Environ. Sci. Technol.*, 2010, **44**, 8692–8697.
31 V. Chandra, J. Park, Y. Chun, J. W. Lee, I.-C. Hwang and K. S. Kim, *ACS Nano*, 2010, **4**, 3979–3986.
32 D. Cohen-Tanugi, L.-C. Lin and J. C. Grossman, *Nano Lett.*, 2016, **16**, 1027–1033.
33 S. K. Kannam, B. Todd, J. S. Hansen and P. J. Daivis, *J. Chem. Phys.*, 2011, **135**, 144701.
34 E. Lauga, M. Brenner and H. Stone, *J. Fluid Mech.*, 2007, 1219–1240.
35 P. A. Thompson and M. O. Robbins, *Physics World*, 1990, **3**, 35.
36 C.-H. Choi, K. J. A. Westin and K. S. Breuer, *ASME 2002 International Mechanical Engineering Congress and Exposition*, 2002, pp. 557–564.
37 S. K. Kannam, B. Todd, J. S. Hansen and P. J. Daivis, *J. Chem. Phys.*, 2012, **136**, 024705.
38 P. A. Thompson and S. M. Troian, *Nature*, 1997, **389**, 360–362.
39 J. J. Thalakkottor and K. Mohseni, *Phys. Rev. E*, 2016, **94**, 023113.
40 M. T. Matthews and J. M. Hill, *Appl. Math. Lett.*, 2008, **21**, 810–813.
41 Z. Li, Y. Wang, A. Kozbial, G. Shenoy, F. Zhou, R. McGinley, P. Ireland, B. Morganstein, A. Kunkel and S. P. Surwade, *et al.*, *Nat. Mater*, 2013, **12**, 925–931.
42 C.-J. Shih, Q. H. Wang, S. Lin, K.-C. Park, Z. Jin, M. S. Strano and D. Blankschtein, *Phys. Rev. Lett.*, 2012, **109**, 176101.
43 J. Rafiee, X. Mi, H. Gullapalli, A. V. Thomas, F. Yavari, Y. Shi, P. M. Ajayan and N. A. Koratkar, *Nat. Mater.*, 2012, **11**, 217–222.
44 R. Raj, S. C. Maroo and E. N. Wang, *Nano Lett.*, 2013, **13**, 1509–1515.
45 G. Tocci, L. Joly and A. Michaelides, *Nano Lett.*, 2014, **14**, 6872–6877.
46 T. Werder, J. H. Walther, R. L. Jaffe, T. Halicioglu and P. Koumoutsakos, *J. Phys. Chem. B*, 2003, **107**, 1345–1352.
47 J. H. Walther, R. Jaffe, T. Halicioglu and P. Koumoutsakos, *J. Phys. Chem. B*, 2001, **105**, 9980–9987.
48 H. A. Zambrano, J. H. Walther and R. L. Jaffe, *J. Chem. Phys.*, 2009, **131**, 241104.
49 W. Xiong, J. Z. Liu, M. Ma, Z. Xu, J. Sheridan and Q. Zheng, *Phys. Rev. E: Stat., Nonlinear, Soft Matter Phys.*, 2011, **84**, 056329.
50 E. Kotsalis, J. Walther and P. Koumoutsakos, *Int. J. Multiphase Flow*, 2004, **30**, 995–1010.
51 M. Sega, M. Sbragaglia, L. Biferale and S. Succi, *Eur. Phys. J. E: Soft Matter Biol. Phys.*, 2015, **38**, 1–7.
52 A. H. Palser, *Phys. Chem. Chem. Phys.*, 1999, **1**, 4459–4464.
53 H. J. C. Berendsen, J. R. Grigera and T. P. Straatsma, *J. Phys. Chem.*, 1987, **91**, 6269–6271.
54 A. Martini, H.-Y. Hsu, N. A. Patankar and S. Lichter, *Phys. Rev. Lett.*, 2008, **100**, 206001.
55 H. J. C. Berendsen, J. P. M. Postma, W. F. van Gunsteren, A. DiNola and J. R. Haak, *J. Chem. Phys.*, 1984, **81**, 3684.
56 L. Xia, C. Choi, S. C. Kothekar and D. Dutta, *Anal. Chem.*, 2015, **88**, 781–788.
57 B. Liu, R. Wu, J. A. Baimova, H. Wu, A. W.-K. Law, S. V. Dmitriev and K. Zhou, *Phys. Chem. Chem. Phys.*, 2016, **18**, 1886–1896.
58 X. Chen, G. Cao, A. Han, V. K. Punyamurtula, L. Liu, P. J. Culligan, T. Kim and Y. Qiao, *Nano Lett.*, 2008, **8**, 2988–2992.
59 K. Ritos, D. Mattia, F. Calabrò and J. M. Reese, *J. Chem. Phys.*, 2014, **140**, 014702.
60 M. D. Ma, L. Shen, J. Sheridan, J. Z. Liu, C. Chen and Q. Zheng, *Phys. Rev. E: Stat., Nonlinear, Soft Matter Phys.*, 2011, **83**, 036316.
61 H. Bruus, *Theoretical microfluidics. Oxford master series in condensed matter physics*, 2008.

62 J. A. Thomas, A. J. McGaughey and O. Kuter-Arnebeck, *Int. J. Therm. Sci.*, 2010, **49**, 281–289.
63 M. Sega, M. Sbragaglia, L. Biferale and S. Succi, *Soft Matter*, 2013, **9**, 8526–8531.
64 A. Maali, T. Cohen-Bouhacina and H. Kellay, *Appl. Phys. Lett.*, 2008, **92**, 053101.
65 M. A. González and J. L. Abascal, *J. Chem. Phys.*, 2010, **132**, 096101.
66 A. Martini, A. Roxin, R. Snurr, Q. Wang and S. Lichter, *J. Fluid Mech.*, 2008, **600**, 257–269.
67 F.-C. Wang and Y.-P. Zhao, *Soft Matter*, 2011, **7**, 8628–8634.
68 R. S. Voronov, D. V. Papavassiliou and L. L. Lee, *J. Chem. Phys.*, 2006, **124**, 204701.
69 N. V. Priezjev and S. M. Troian, *Phys. Rev. Lett.*, 2004, **92**, 018302.
70 R. Saito, R. Matsuo, T. Kimura, G. Dresselhaus and M. Dresselhaus, *Chem. Phys. Lett.*, 2001, **348**, 187–193.
71 L. Girifalco, M. Hodak and R. S. Lee, *Phys. Rev. B: Condens. Matter Mater. Phys.*, 2000, **62**, 13104.
72 E. Lauga and H. A. Stone, *J. Fluid Mech.*, 2003, **489**, 55–77.
73 K. Falk, F. Sedlmeier, L. Joly, R. R. Netz and L. Bocquet, *Nano Lett.*, 2010, **10**, 4067–4073.
74 Y.-C. Liu, J.-W. Shen, K. E. Gubbins, J. D. Moore, T. Wu and Q. Wang, *Phys. Rev. B: Condens. Matter Mater. Phys.*, 2008, **77**, 125438.

